RESEARCH ARTICLE | SEPTEMBER 27 2023

High expectations on phase locking: Better quantifying the concentration of circular data FREE

Ralph G. Andrzejak ✉ (iD) ; Anaïs Espinoso (iD) ; Eduardo García-Portugués (iD) ; Arthur Pewsey (iD) ;
Jacopo Epifanio (iD) ; Marc G. Leguia (iD) ; Kaspar Schindler (iD)

 Check for updates

CrossMark

View
Online

Export
Citation

Articles You May Be Interested In

Outlier detection in a new half-circular distribution

AIP Conference Proceedings (October 2015)

Logistic regression for circular data

AIP Conference Proceedings (May 2017)

Melodic expectancy in infancy

J Acoust Soc Am (October 1999)

High expectations on phase locking: Better quantifying the concentration of circular data

Ralph G. Andrzejak,[1,a] [ID] Anaïs Espinoso,[1,2] [ID] Eduardo García-Portugués,[3] [ID] Arthur Pewsey,[4] [ID]
Jacopo Epifanio,[1] [ID] Marc G. Leguia,[1] [ID] and Kaspar Schindler[5] [ID]

AFFILIATIONS

[1] Department of Information and Communication Technologies, Universitat Pompeu Fabra, Carrer Roc Boronat 138,
08018 Barcelona, Catalonia, Spain
[2] Institute for Bioengineering of Catalonia (IBEC), The Barcelona Institute of Science and Technology, Carrer Baldiri Reixac 10-12,
08028 Barcelona, Catalonia, Spain
[3] Department of Statistics, Universidad Carlos III de Madrid, Av. de la Universidad 30, 28911 Leganés, Madrid, Spain
[4] Mathematics Department, Escuela Politécnica, Universidad de Extremadura, Av. de la Universidad s/n, 10003 Cáceres, Spain
[5] Sleep Wake Epilepsy Center, Department of Neurology, Inselspital, Bern University Hospital, University of Bern, Bern 3010,
Switzerland

[a] Author to whom correspondence should be addressed: ralph.andrzejak@upf.edu

ABSTRACT

The degree to which unimodal circular data are concentrated around the mean direction can be quantified using the mean resultant length, a measure known under many alternative names, such as the phase locking value or the Kuramoto order parameter. For maximal concentration, achieved when all of the data take the same value, the mean resultant length attains its upper bound of one. However, for a random sample drawn from the circular uniform distribution, the expected value of the mean resultant length achieves its lower bound of zero only as the sample size tends to infinity. Moreover, as the expected value of the mean resultant length depends on the sample size, bias is induced when comparing the mean resultant lengths of samples of different sizes. In order to ameliorate this problem, here, we introduce a re-normalized version of the mean resultant length. Regardless of the sample size, the re-normalized measure has an expected value that is essentially zero for a random sample from the circular uniform distribution, takes intermediate values for partially concentrated unimodal data, and attains its upper bound of one for maximal concentration. The re-normalized measure retains the simplicity of the original mean resultant length and is, therefore, easy to implement and compute. We illustrate the relevance and effectiveness of the proposed re-normalized measure for mathematical models and electroencephalographic recordings of an epileptic seizure.

Real-world data often depend on circular variables, a typical example being average wind speed as a function of compass needle direction. Circular data often show concentration around some central value, such as the elevated incidence of infectious diseases in a certain season. The classical measure of the concentration of unimodal circular data is the mean resultant length,[1–3] which is applied in many scientific fields.[4–40] Given a certain value of the mean resultant length obtained for experimental or observational data, statistical tests can be used to assess its significance under the null hypotheses of uniformity or specified circular location.[1–3,41] However, the value itself can be difficult to interpret. The reason is that for data drawn from the circular uniform distribution, the expected value of the mean resultant length for a finite number of observations is non-zero and increases with decreasing sample size. This sample size dependence can be misleading. When the mean resultant length is used to assess synchronization, for example, a small network of fully independent nodes can erroneously be concluded to be more synchronized than a bigger network for which coupling between nodes actually induces some coherence. To address this problem, here, we propose a simple re-normalization of the mean resultant length. Whatever the sample size, our re-normalized measure has an expected value of essentially zero for data drawn from the circular uniform distribution and attains its upper bound of one, corresponding to maximal concentration, when all of the data take the same value. Thus, the re-normalized mean resultant

length provides a more informative measure of the concentration of circular data than the original mean resultant length, without diminishing its universal applicability, simplicity, and ease of implementation.

I. INTRODUCTION

The mean resultant length plays a central role in circular statistics[1–3] and is referred to by various names in different scientific communities, such as the Kuramoto order parameter,[42] phase coherence,[4] phase stack,[28] phase synchronization index,[7] phase locking value,[8] or mean phase coherence.[9] Several generalizations, such as, for example, the triplet synchronization index,[43] exist. Applications of the mean resultant length are so numerous and widespread across scientific disciplines that any attempt to compile a halfway comprehensive summary would fill numerous pages. We, therefore, restrict ourselves to reference some examples from neuroscience,[4–6] neurology,[7–13] cardiology,[14,15] other fields of medicine,[16,17] psychology,[18,19] biomedical engineering,[20,21] biology,[22,23] ecology,[24,25] climatology,[26,27] seismology,[28,29] chemistry,[30,31] physics,[32,33] astronomy,[34,35] computer science,[36,37] the study of mathematical models,[38,39] and last but not least the classical work of Rayleigh on acoustics.[40]

We review the definition of the mean resultant length and illustrate the problems caused by its sample size dependence in Sec. II. In Sec. III, we propose our re-normalized mean resultant length. After using mathematical models in Secs. II and III to illustrate the relevance and effectiveness of our re-normalized measure under controlled conditions, in Sec. IV, we apply it in an analysis of an electroencephalographic (EEG) recording of an epileptic seizure to illustrate its application to real-world data. In Sec. V, we briefly consider complementary approaches and the unbiased estimate of squared mean resultant length. As we discuss in Sec. VI, our aim is not to address the statistical testing of circular concentration, but to introduce the re-normalized mean resultant length as a measure with improved interpretability, which is particularly useful when comparing levels of concentration across experiments with different sample sizes.

II. CLASSICAL MEAN RESULTANT LENGTH

Let Θ_j, for $j = 1, \ldots, n$, denote a random sample of size n from some circular distribution on $[0, 2\pi)$. A pertinent example would be the phases of n oscillators at a certain time t. Indeed, for the sake of brevity and without loss of generality, henceforth, we generally refer to the Θ_j's as phases. In some derivations below, we assume that the Θ_j's are n independent and identically distributed (iid) random variables from the circular uniform distribution. Whenever this assumption is made, we use the expression $\Theta_1, \ldots, \Theta_n \sim \mathcal{CU}$. Whatever the circular distribution from which the Θ_j's were sampled, the mean resultant length can be defined in two equivalent ways (see, e.g., Sec. 1.3.1 in Ref. 3),

$$\bar{R}_n := \frac{1}{n} \left| \sum_{j=1}^{n} e^{i\Theta_j} \right|, \tag{1}$$

where $i = \sqrt{-1}$ and $| \cdot |$ denotes modulus, or $\bar{R}_n := \|\bar{\mathbf{X}}\|$, where $\bar{\mathbf{X}} := \frac{1}{n} \sum_{j=1}^{n} (\cos \Theta_j, \sin \Theta_j)'$ and $\| \cdot \|$ is the Euclidean norm on $\mathbb{R}^2$. The notation $\bar{R}_n$ is used in order to clarify that the *sample* mean resultant length determined for a finite number of n phases is being referred to, as opposed to its *population* counterpart $\left(\left| \mathbf{E} \left[e^{i\Theta_1} \right] \right|$ if the sample is iid$\right)$ that summarizes the concentration of a circular distribution from which the phases were drawn. Clearly, $\bar{R}_n$ attains its upper bound of one if and only if all of the Θ_j are equal. The lower bound of $\bar{R}_n$ is zero, obtained when $\bar{\mathbf{X}} = \mathbf{0}$. This occurs, for instance, when the data distribution is antipodally (or twofold) symmetric: for example, an even number of phases with $\Theta_{j+1} = \Theta_j + \pi$ for $j = 1, 3, \ldots, n - 1$. However, for such data, and more generally for ℓ-fold symmetric and some other forms of reflectively symmetric data, $\bar{R}_n$ is no longer a measure of concentration but rather a measure of symmetry. As is well known, and as we illustrate below, for finite n, the expected value of $\bar{R}_n$ is not zero for $\Theta_1, \ldots, \Theta_n \sim \mathcal{CU}$.

Consider the circular uniform case with $\Theta_1, \ldots, \Theta_n \sim \mathcal{CU}$. Being a function of n random variables, $\bar{R}_n$ is itself a random variable, with a probability density function that does not admit a closed form (see Sec. 4.1.1 in Ref. 1). Due to the central limit theorem, in the limit as $n \to \infty$, the density of $\bar{R}_n$ reduces to the Dirac delta function, as then $\bar{R}_n = 0$ with probability one. The situation is more complicated for finite n, and we use the following example of two dynamical systems, A and B, to illustrate an important problem of interpretation that can occur. To define system A, we use $n_A = 5$ independent harmonic oscillators with the phases $\phi_j(t)$ governed by

$$\dot{\phi}_j(t) = \omega_{A,j} \tag{2}$$

for $j = 1, \ldots, n_A$, where the dot denotes differentiation with respect to time and $\omega_{A,j}$ is the natural frequency of oscillator j. For system B, we use a standard Kuramoto model[42] for a network of $n_B = 10$ all-to-all coupled oscillators with phases $\psi_j(t)$. For $j = 1, \ldots, n_B$, the temporal evolution of the phases is determined by

$$\dot{\psi}_j(t) = \omega_{B,j} - \frac{K(t)}{n_B} \sum_{k=1}^{n_B} \sin \left(\psi_j(t) - \psi_k(t) \right), \tag{3}$$

where $\omega_{B,j}$ denotes the natural frequency of oscillator j and $K(t)$ is a time-dependent coupling. Starting from initial conditions of independent and identically distributed observations from the circular uniform distribution, both systems are integrated using a fourth-order Runge–Kutta scheme with a sampling time of $\Delta t = 0.05$ during a total of 2500 time units. The coupling is set to $K(t) = 0$ for $0 \leq t < 1250$ and $K(t) = 2.7$ for $1250 < t \leq 2500$. Both $\omega_{A,j}$ and $\omega_{B,j}$ are drawn at random from a normal distribution with mean 6.0 and standard deviation 1.25 radians per time unit (see Appendix A).

For any time t, the phases $\phi_j(t)$ and $\psi_j(t)$ are then used as Θ_j in Eq. (1) to calculate the mean resultant length $\bar{R}_n$ for systems A and B as a function of t [Fig. 1(a)]. A naïve interpretation of these results is that during the entire time period, both systems have some intermediate degree of phase locking across oscillators. The phase locking of system B increases at 1250 but does not reach the level of system A. If we were to regard these interpretations as evidence of coupling within systems A and B, our conclusion would be quite wrong. The reason for this misinterpretation is easily explained. To begin with, being generated by Eqs. (2) and (3), the phases evolve

deterministically. However, at any moment in time, during which the oscillators evolve independently, they can be regarded as a set of independent and identically distributed observations from a circular uniform distribution. This means that in the absence of coupling, the assumption $\Theta_1, \ldots, \Theta_n \sim \mathcal{CU}$ holds. Accordingly, during the entire 2500 time units, the results for system A fluctuate around a non-zero offset given by the expected value of $\bar{R}_n$ for $\Theta_1, \ldots, \Theta_n \sim \mathcal{CU}$ with $n = 5$. During the first 1250 time units, the results for system B fluctuate around the corresponding expected value of $\bar{R}_n$ for $n = 10$. As one can see in Fig. 1(a), the expected value of $\bar{R}_n$ is higher for $n = 5$ than for $n = 10$. Once the coupling for system B is activated in the second 1250 time units, the assumption $\Theta_1, \ldots, \Theta_n \sim \mathcal{CU}$ is no longer fulfilled for this dynamical system. The coupling leads to a certain degree of dependence of the phases across oscillators. This results in an increase of the $\bar{R}_n$ values of system B, however, without reaching the values of the uncoupled system A. Hence, the smaller-sized uncoupled system A has higher values of the mean resultant length than the larger-sized system B, irrespective of whether the oscillators of B are coupled or not.

To further illustrate the sample size dependence of the mean resultant length $\bar{R}_n$, we consider results for the von Mises distribution (see, e.g., Sec. 3.5.4 in Ref. 1). This continuous uni-modal circular distribution has two parameters, the mean direction $\mu_0 \in [0, 2\pi)$ and the concentration parameter $\kappa > 0$. As $\kappa \to 0$, the von Mises distribution converges to a circular uniform distribution. As κ increases, the distribution is increasingly concentrated around the mean direction μ_0. Figure 1(b) shows the average mean resultant length $\bar{R}_n$ as a function of κ for a range of values of n. For high κ values, $\bar{R}_n$ converges to its upper limit of one, regardless of n. However, for smaller κ, the average $\bar{R}_n$ curves for different n diverge from one another. In the limit of a circular uniform distribution ($\kappa \to 0$), the curves converge to different offsets. This further illustrates that for independent identically distributed observations from the circular uniform distribution ($\Theta_1, \ldots, \Theta_n \sim \mathcal{CU}$), the expected value of the mean resultant length calculated for a finite number of n observations is non-zero and depends on n.

III. RE-NORMALIZED MEAN RESULTANT LENGTH

Having understood what causes the problems illustrated in Figs. 1(a) and 1(b), when re-normalizing $\bar{R}_n$, we first require the expected value of $\bar{R}_n$ for phases without a preferred direction. More precisely, we need the expected value $\mathsf{E}[\bar{R}_n]$ for $\Theta_1, \ldots, \Theta_n \sim \mathcal{CU}$. Here, the expectation is taken across independent observations of $\bar{R}_n$, each resulting from n phases. As shown in Appendix B, we can use the following fast-converging asymptotic approximation:

$$\mathsf{E}[\bar{R}_n] \approx \gamma_n := \frac{1}{2}\sqrt{\frac{\pi}{n}}. \tag{4}$$

Using this approximation, we first center $\bar{R}_n$ by subtracting γ_n and then divide by the maximum value of the resulting centered measure (see, for example, Ref. 44 and references therein for instances of this type of re-normalization), so as to obtain the re-normalized mean resultant length,

$$\bar{T}_n := \frac{\bar{R}_n - \gamma_n}{1 - \gamma_n}. \tag{5}$$

For $\Theta_1, \ldots, \Theta_n \sim \mathcal{CU}$, $\mathsf{E}[\bar{T}_n]$ is essentially zero for $n \geq 2$. This is fundamentally different from $\mathsf{E}[\bar{R}_n]$ for $\Theta_1, \ldots, \Theta_n \sim \mathcal{CU}$, which strongly depends on n and, even for large n, can be substantially higher than zero [see Eq. (4) and Figs. 1(a) and 1(b)]. Both measures have the same well-defined upper limit: if and only if all n values Θ_j are equal, $\bar{T}_n = \bar{R}_n = 1$. The lower limit of $\bar{T}_n$ is obtained for two antipodal phases ($\Theta_2 = \Theta_1 + \pi$) and is given by $-\gamma_2/(1 - \gamma_2) = -1.679$ to three decimal places.

Figure 1(c) shows that the re-normalized mean resultant length $\bar{T}_n$ resolves the problem detected for the original mean resultant length $\bar{R}_n$ in Fig. 1(a). The values of $\bar{T}_n$ for system A fluctuate around zero during the entire time interval. The same is found for system B during the first 1250 time units. In contrast, $\bar{T}_n$ rises to a non-zero average value for system B during the second 1250 time units. If these results were used to draw conclusions about the couplings in the two dynamics, those conclusions would be correct. Only the oscillators of system B are mutually coupled and only during the second 1250 time units. Furthermore, Fig. 1(d) shows that $\bar{T}_n$ provides a solution to the problem with the use of $\bar{R}_n$ illustrated in Fig. 1(b). The re-normalized measure $\bar{T}_n$ converges to zero and one for low and high values, respectively, of the concentration parameter κ of the von Mises distribution. For intermediate κ values, only a weak dependence on n is found. We also investigated the results of Figs. 1(a) and 1(c) for stochastic versions of the dynamical systems from Eqs. (2) and (3), where we added dynamical Gaussian white noise. We considered several noise variances, all smaller than the signal variance to have a meaningful identifiable trend. The same qualitative results of Figs. 1(a) and 1(c) were obtained, and hence, the results are not shown here.

IV. APPLICATION TO RECORDING OF AN EPILEPTIC SEIZURE

To illustrate the relevance of our re-normalized measure for the analysis of real-world data, we present an application to an EEG recording of an epileptic seizure. This multichannel recording was part of the diagnostic testing carried out for a patient with pharmacoresistant focal-onset epilepsy and allowed the clinicians to localize the seizure onset zone, i.e., the area of the patient's brain where the first signal changes of the seizure were detected. Based on the localization of the seizure onset zone along with the overall results of the diagnostic testing, the clinicians delineated the brain area, which was then to be removed by epilepsy surgery. After this surgery, the patient became seizure-free. Due to characteristics of this recording, the results of the diagnostics, and the positive surgery outcome of the patient, we can use the following notion of focal and non-focal dynamics. There were 11 EEG recording channels placed in close proximity to the seizure onset zone, capturing the focal dynamics. For the non-focal dynamics, we randomly selected five EEG channels, which recorded from areas that were not involved in the seizure at its onset. We used the analytic signal concept based on the Hilbert transform to compute the instantaneous phases from band-pass filtered EEG signals. This resulted in 11 and 5 temporal phase profiles for the focal and non-focal dynamics, respectively. (For further details of the EEG recording and data pre-processing, see Appendix C.) For any fixed time t, and separately for the focal and non-focal dynamics, the phases were used as Θ_j in Eq. (1) to
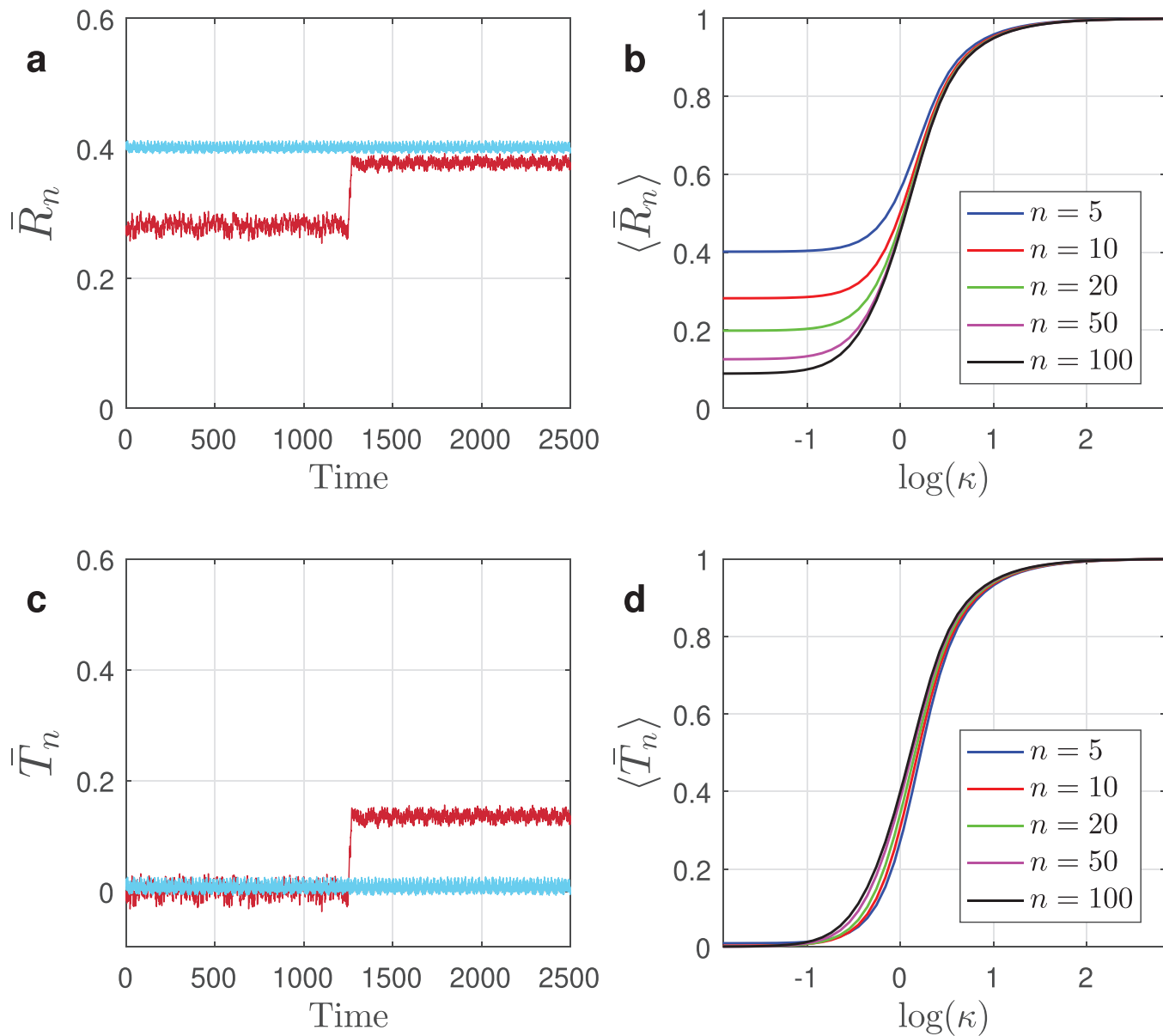
FIG. 1. (a) Dependence of $\bar{R}_n$ [Eq. (1)] on time for dynamical systems A (blue) and B (red). Both curves are smoothed with a moving average of 20 time units (see Appendix A). Note that this graph is not scaled to the upper limit of $\bar{R}_n$, which is one. Furthermore, recall that both systems are started from initial conditions of independent and identically distributed observations from the circular uniform distribution, and at time $t = 0$, all oscillators in both systems are independent. Accordingly, there are no initial transients. (b) Dependence of $\bar{R}_n$ on the concentration parameter κ of a von Mises distribution with mean direction $\mu_0 = \pi$. The different curves show the sample means of $\bar{R}_n$ across 10^9 sets of n observations each (n is indicated in the legend). (c) Same as panel (a) but for $\bar{T}_n$ [Eq. (5)]. (d) Same as panel (b) but for $\bar{T}_n$.

calculate the mean resultant length $\bar{R}_n$ and the re-normalized mean resultant length $\bar{T}_n$. Performing this analysis for all t included in the EEG recording yielded the temporal profiles shown in Fig. 2.

Before and after the seizure, the mean resultant length $\bar{R}_n$ attains similar levels for the focal and non-focal dynamics [Fig. 2(a)].

In contrast, values of the re-normalized mean resultant length $\bar{T}_n$ are clearly higher for the focal dynamics as compared to the non-focal dynamics [Fig. 2(c)]. The results for $\bar{T}_n$ are more meaningful than those for $\bar{R}_n$, because the focal dynamics are consistently reported to show a higher degree of synchronization than
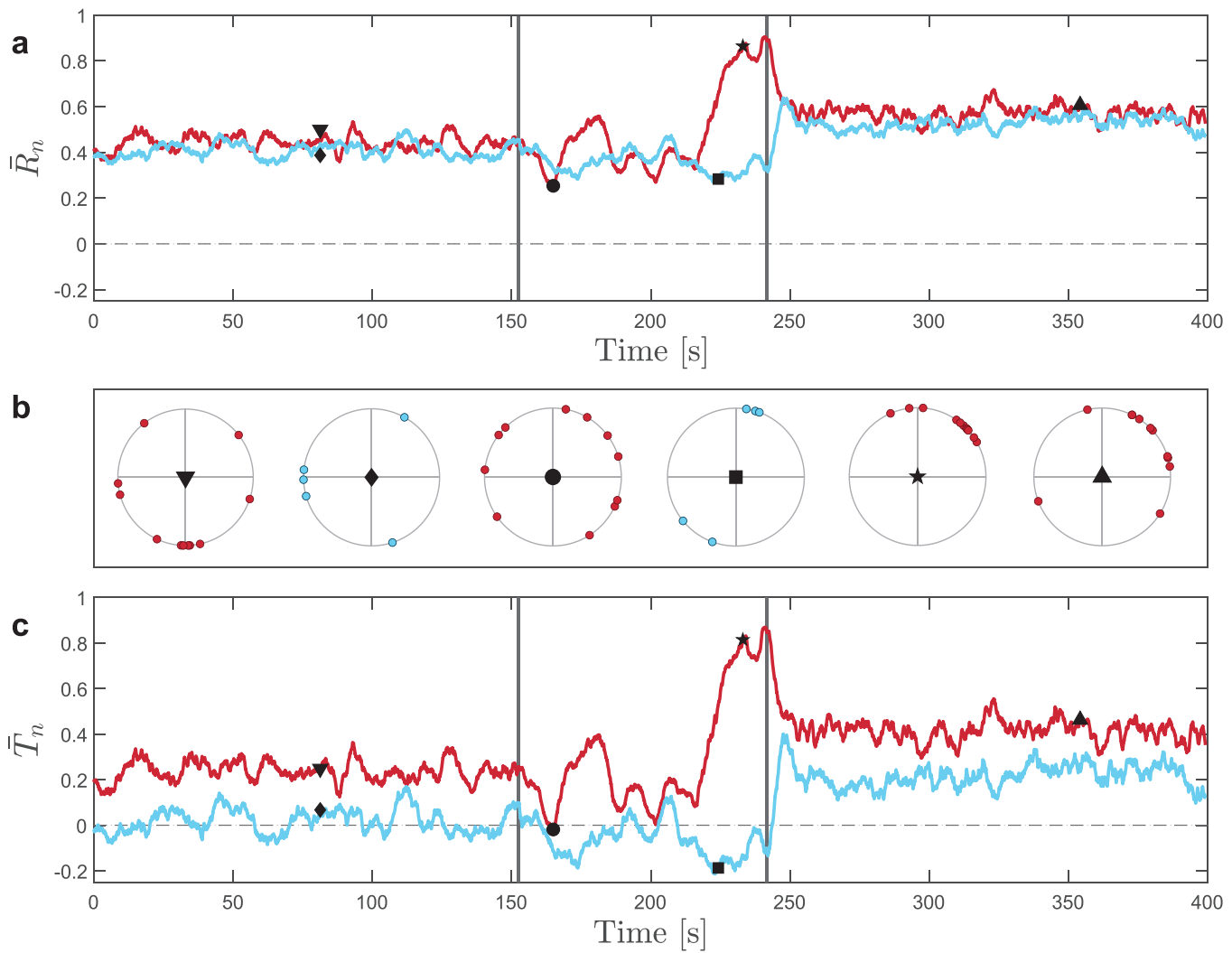
FIG. 2. (a) Dependence of $\bar{R}_n$ on time for the focal dynamics (red) and non-focal dynamics (blue), captured by 11 and 5 EEG recording channels, respectively. (b) Exemplary snapshots of the phases drawn schematically on a unit circle. The symbols in the center of the circles identify the corresponding curve and the time point in panels (a) and (c). (c) Same as panel (a) but for $\bar{T}_n$. All curves in (a) and (c) are smoothed with a moving average of 5 s.

the non-focal dynamics during the periods, which do not include seizures.[9,10,13,45–55] Accordingly, such quantitative EEG analysis may support clinicians in the localization of the seizure onset zone. We should furthermore note that before the seizure, the $\bar{T}_n$ values for the non-focal dynamics remain close to zero. Accordingly, the underlying $\bar{R}_n$ values apparently only reflect the high value expected for the five instantaneous phases used for the non-focal dynamics. During the seizure, at around 170 and 220 s, the non-focal $\bar{T}_n$ values show two prominent drops below zero. This can be explained by the approximately antipodal arrangement of the phases during these periods [see insets in Fig. 2(b)]. The value of γ_n used to calculate $\bar{T}_n$ is based on the assumption that the phases are independent observations from the circular uniform distribution. For an approximately

antipodal arrangement, $\bar{R}_n < \gamma_n$ and therefore, $\bar{T}_n < 0$. Again, the measure $\bar{T}_n$ is more informative than $\bar{R}_n$. Due to the lack of a reference level in $\bar{R}_n$, it is not possible to detect when its values fall below the one expected for uniformly distributed phases.

Regarding the $\bar{T}_n$ profile of the focal dynamics during the seizure, we see a pronounced drop shortly after the onset of the seizure, followed by a first pronounced peak and a sequence of drops. A very prominent peak is found at the end of the seizure. This temporal profile can be detected in both $\bar{R}_n$ and $\bar{T}_n$. However, only the measure $\bar{T}_n$ allows us to clearly conclude that for the focal dynamics, the minima during the seizure do not fall below the levels expected for uniformly distributed phases. Overall, this temporal evolution of the re-normalized mean resultant length $\bar{T}_n$ is in

03 October 2023 09:46:41

line with previous findings on the dynamics of epileptic seizures. While seizures are classically considered to reflect abnormal excessive or synchronous neuronal activity,[56] it has been shown that, apart from synchronization, de-synchronization is also important for seizure dynamics.[57–62] In particular, as reviewed in Ref. 63, de-synchronization is often observed preceding seizures or during their early stages, while high levels of synchronization are commonly found toward the end of seizures.

V. COMPLEMENTARY APPROACHES

The fact that the expected value of $\bar{T}_n$ for n independent identically distributed observations from the circular uniform distribution $(\Theta_1, \ldots, \Theta_n \sim \mathcal{CU})$ is not exactly zero is due to the fact that γ_n is only an approximation to $\mathbf{E}[\bar{R}_n]$. However, as shown numerically (see Appendix B), the deviation of $\mathbf{E}[\bar{T}_n]$ from zero is relatively small compared to its standard deviation under $\Theta_1, \ldots, \Theta_n \sim \mathcal{CU}$. For ease of implementation, therefore, it would seem reasonable to neglect this deviation. If deemed necessary, however, the deviation from zero can be addressed at little extra cost. Monte Carlo estimated values of $\mathbf{E}[\bar{R}_n]$ can be used for small $n \leq n_0$, while γ_n [Eq. (4)] can be used for large $n > n_0$. The threshold n_0 can be set according to the required level of accuracy. For these estimated values and accuracies, see Table II in Appendix B and the supplementary material.

Another alternative to $\bar{R}_n$ and $\bar{T}_n$ is to use the squared mean resultant length, which follows from Eq. (1) and can be written as

$$\bar{R}_n^2 := \frac{1}{n^2} \left| \sum_{j=1}^{n} e^{i\Theta_j} \right|^2. \tag{6}$$

It is well known and can be shown with basic calculus that $\mathbf{E}[\bar{R}_n^2] = 1/n$ for $\Theta_1, \ldots, \Theta_n \sim \mathcal{CU}$. This value is exact; no approximation is required. One can proceed analogously to Eq. (5) and define

$$\bar{T}_n^2 := \frac{\bar{R}_n^2 - 1/n}{1 - 1/n}. \tag{7}$$

In contrast to $\bar{T}_n$, the quantity $\bar{T}_n^2$ has an expected value of exactly zero for $\Theta_1, \ldots, \Theta_n \sim \mathcal{CU}$. However, for the squared mean resultant length, a more general solution exists. By turning it into a U-statistic,[64] it is straightforward to unbias $\bar{R}_n^2$. In particular, this follows from Eq. 4.7.3 in Ref. 1. References 65 and 66 used this unbiased version of $\bar{R}_n^2$.

We emphasize again that γ_n, and, therefore, $\bar{T}_n$, assume that the data form a random sample from the circular uniform distribution. We are not aware of any closed-form expressions for $\mathbf{E}[\bar{R}_n]$ when the underlying distribution is not circular uniform. However, values of $\mathbf{E}[\bar{R}_n]$ can be estimated straightforwardly and precisely, either using large samples drawn from known distributions or using non-parametric bootstrap methods when the underlying distribution is unknown. These values can be used to define measures analogous to $\bar{T}_n$ when the underlying distribution is known, or assumed, not to be circular uniform.

VI. DISCUSSION

There exist well-developed inferential methods for circular data, in particular, for testing the null hypothesis of uniformity on the circle (e.g., Refs. 1–3 and 41). However, our aim in re-normalizing $\bar{R}_n$ has been to improve its interpretation and, thus, its use in exploratory data analysis, not to address the issue of statistical inference for the population mean resultant length or testing for circular uniformity. There exists other relevant work regarding the mean resultant length $\bar{R}_n$ and its statistical properties in applications to real-world data. That work addresses the impact of noise,[67,68] non-stationarity,[68] and results expected when the data are assumed to come from certain non-uniform circular distributions,[5] to name just three contexts. The main findings from them carry over readily to $\bar{T}_n$ since it is simply a re-normalization of $\bar{R}_n$. Nonetheless, that re-normalization is essential. The expected value of $\bar{T}_n$ for n independent and identically distributed observations from the circular uniform distribution $(\Theta_1, \ldots, \Theta_n \sim \mathcal{CU})$ has two important properties. First, it is essentially zero. This reduces the risk of false positive conclusions of concentration of the circular variable around some central value. Second, its expectation is essentially independent of the sample size, n, an important feature that facilitates the comparison of concentration across samples with different sizes. A further advantage of $\bar{T}_n$ over $\bar{R}_n$ is that it is only weakly dependent on the sample size for partially concentrated data, as we have illustrated with observations from von Mises distributions. In closing, we note that while one of our models and the application to real-world data used time-dependent phases, the scope of this approach is much wider. The re-normalized mean resultant length can be applied to any type of circular data to which the classical mean resultant length can be applied (e.g., Refs. 4–40).

SUPPLEMENTARY MATERIAL

See the supplementary material for tables analogous to Table II in Appendix B but for $n = 2, \ldots, 100$.

AUTHOR DECLARATIONS
Conflict of Interest

The authors have no conflicts to disclose.

Author Contributions

Ralph G. Andrzejak: Conceptualization (lead); Data curation (equal); Formal analysis (lead); Investigation (lead); Validation

(lead); Visualization (lead); Writing – original draft (lead); Writing – review & editing (lead). **Anaïs Espinoso:** Conceptualization (equal); Data curation (equal); Formal analysis (equal); Visualization (lead); Writing – original draft (equal); Writing – review & editing (equal). **Eduardo García-Portugués:** Conceptualization (equal); Formal analysis (equal); Investigation (lead); Validation (lead); Writing – review & editing (lead). **Arthur Pewsey:** Investigation (lead); Validation (lead); Writing – review & editing (lead). **Jacopo Epifanio:** Writing – original draft (equal); Writing – review & editing (equal). **Marc G. Leguia:** Writing – original draft (equal); Writing – review & editing (equal). **Kaspar Schindler:** Data curation (lead); Validation (lead); Writing – review & editing (equal).

DATA AVAILABILITY

The data that support the findings of this study are openly available in the electronic library repository of the Universitat Pompeu Fabra at https://doi.org/10.34810/data845 (see Ref. 69).

APPENDIX A: NATURAL FREQUENCIES OF DYNAMICAL SYSTEMS A AND B

Consider the dynamical system A introduced in Sec. II, which is just a set of independent oscillators. Accordingly, all oscillators rotate at their constant natural frequencies $\omega_{A,j}$. Because these frequencies are drawn at random and are not integer multiples of each other, groups of oscillators will form in narrow phase ranges and directly resolve again in a quasi-random manner. This leads to fast fluctuations of the mean resultant length and the re-normalized mean resultant length. The same holds true for system B in the absence of coupling $[K(t) = 0]$. To dampen these fluctuations, the curves in Figs. 1(a) and 1(c) are smoothed by a moving average filter. Depending on the particular random sample of natural frequencies $\omega_{A,j}$ and $\omega_{B,j}$, the aforementioned formation and dissolving of subgroups of oscillators takes place on longer time scales, leading to slow modulation in the $\bar{R}_n$ and $\bar{T}_n$ curves. The examples shown in Figs. 1(a) and 1(c) have the frequencies given in Table I, for which no slow modulation is obtained.

APPENDIX B: EXPECTED VALUE OF THE MEAN RESULTANT LENGTH

Throughout this Appendix B, we assume that the phases Θ_j for $j = 1, \ldots, n$ are iid circular uniform random variables $(\Theta_1, \ldots, \Theta_n \sim \mathcal{CU})$. As indicated in the main text, one can readily show that $\mathsf{E}[\bar{R}_n^2] = 1/n$. In contrast, for $\mathsf{E}[\bar{R}_n]$, no closed-form

expression exists for all n. However, a standard application of the (multivariate) central limit theorem shows that, as $n \to \infty$, $\sqrt{2n}\bar{\mathbf{X}}$ is asymptotically distributed as the standard bivariate normal $\mathcal{N}_2(\mathbf{0}, \mathbf{I}_2)$, where $\bar{\mathbf{X}}$ was defined after Eq. (1) and $\mathbf{I}_2$ is the 2×2 identity matrix (the asymptotic variance–covariance matrix). An application of the continuous mapping theorem with $\| \cdot \|$, thus, implies that $\sqrt{2n}\|\bar{\mathbf{X}}\| = \sqrt{2n}\bar{R}_n$ is asymptotically distributed as $\|\mathcal{N}_2(\mathbf{0}, \mathbf{I}_2)\|$, that is, as a chi random variable with two degrees of freedom (χ_2). Since $\mathsf{E}[\chi_2] = \sqrt{2\pi}/2$, then $\lim_{n \to \infty} \sqrt{2n}\mathsf{E}[\bar{R}_n] = \sqrt{2\pi}/2$, from which it follows that

$$\mathsf{E}[\bar{R}_n] \approx \frac{1}{2}\sqrt{\frac{\pi}{n}} =: \gamma_n. \tag{B1}$$

For small n, the distribution of $\sqrt{2n}\bar{R}_n$ deviates strongly from the χ_2 distribution [Figs. 3(a)–3(d)]. Nevertheless, as can be verified numerically and is shown in Table II, the expected value of $\bar{R}_n$ remains close to γ_n even for small n. Therefore, even for small sample sizes, Eq. (B1) remains a remarkably good approximation [Fig. 3(e), Table II, columns 2–4], and consequently, $\mathsf{E}[\bar{T}_n]$ remains close to zero [Fig. 3(f), Table II, column 5]. Even though the asymptotic distribution of $\bar{R}_n$ was identified by Lord Rayleigh in 1880,[40] we have not been able to find systematic analysis of its small sample accuracy like that presented in Table II and Fig. 3. We point out a notable exception: $\mathsf{E}[\bar{R}_2] = 2/\pi$ is known exactly (see Eq. 4.4.10 in Ref. 1) due to the univariate nature of the problem.

APPENDIX C: INTRACRANIAL ELECTROENCEPHALOGRAPHIC RECORDINGS

The electroencephalographic (EEG) recording analyzed in Sec. IV was acquired at the Inselspital Bern (Bern, Switzerland). Intracranial EEG recordings for localizing the seizure onset zone have to be tailored to the individual patient. They are highly personalized, and thus, often, different numbers of electrodes are used for different patients.[70] The recording was obtained using eight intracranial electrodes with a total of 64 channels, with 11 of them located in close proximity to the seizure onset zone as determined by an experienced epileptologist (K.S.). An extracranial reference electrode placed between 10/20 positions Fz and Pz was used. The data were recorded at a sampling rate of 512 Hz, and EEG signals were then re-referenced against the median of all the channels free of permanent artifacts as judged by visual inspection. We filtered the signals between 4 and 30 Hz using a finite impulse response (FIR) band-pass filter prior to the analysis. The reference scheme and the filter setting were taken from an earlier analysis of a larger data set, including the recording analyzed here.[71] No prominent artifacts were detected in this recording.

TABLE I. Frequencies used in Eqs. (2) and (3).

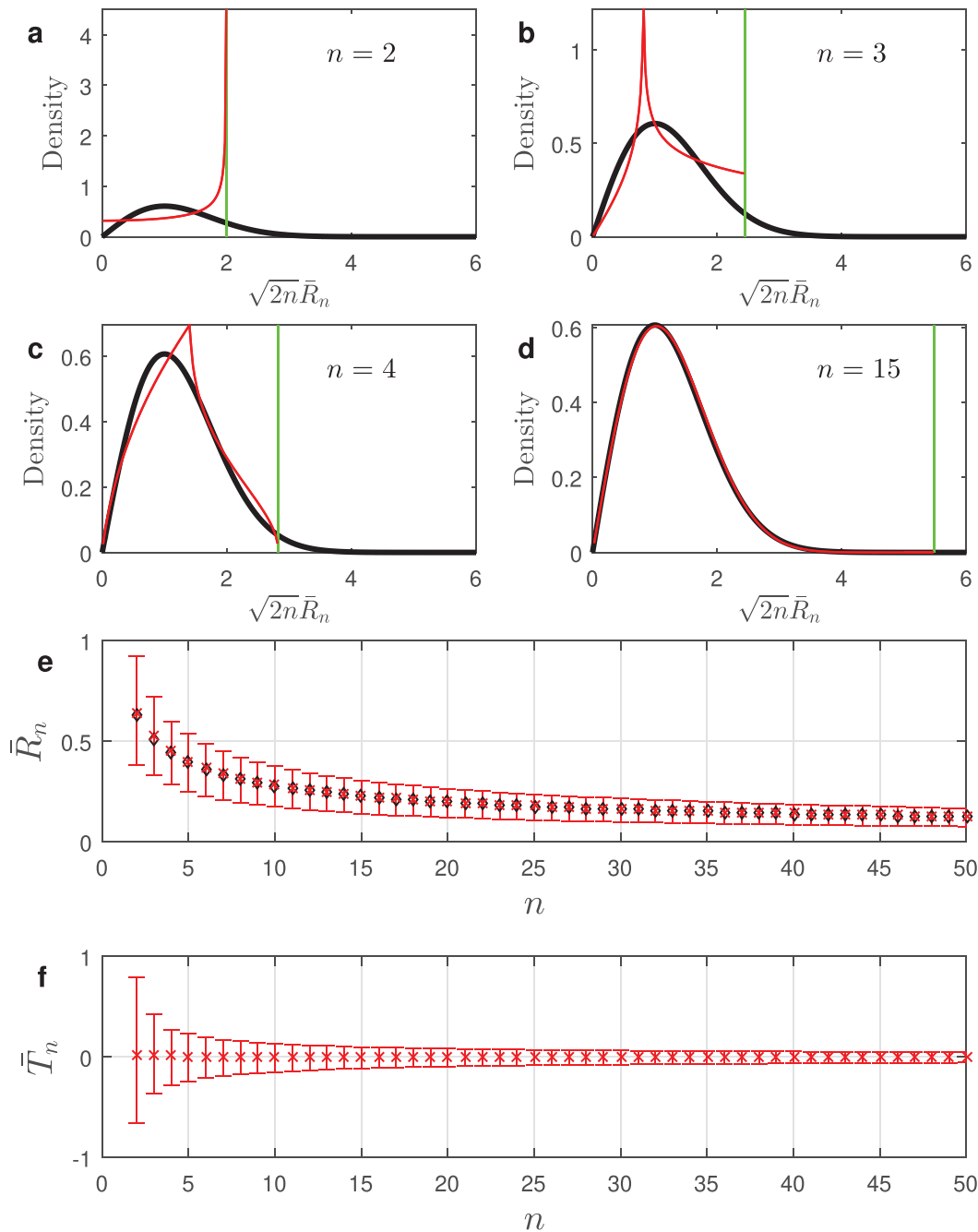| j	1	2	3	4	5	6	7	8	9	10
$\omega_{A,j}$	5.57	10.17	3.12	19.18	5.89	...	...	...	...	...
$\omega_{B,j}$	5.19	8.95	3.16	0.45	0.71	1.71	1.11	7.78	3.79	13.33

FIG. 3. Numerical approximation of the densities of $\bar{R}_n$ and $\bar{T}_n$. For each n, we generated $N = 10^9$ circular uniform random samples of size n. For each of the N samples, the values of $\bar{R}_n$ and $\bar{T}_n$ were then calculated. (a)–(d) Probability density functions of the χ_2 distribution (black) and the estimated probability density function of $\sqrt{2n}\bar{R}_n$ using a fine frequency polygon (red). The green lines mark the abscissa value $\sqrt{2n}$, the upper limit of the support of $\sqrt{2n}\bar{R}_n$. (e) Red: Dependence of $\bar{R}_n$ on n. The error bars mark the sample mean (central cross) along with the 25th and 75th percentile of each distribution of N observations. The fact that the ordinate values of the red crosses and the black diamonds (γ_n) can hardly be distinguished shows that γ_n is a very close approximation to $\mathbf{E}[\bar{R}_n]$ (see the fourth column of Table II for the remaining deviations). (f) Dependence of $\bar{T}_n$ on n, with the same layout as for (e). It can be seen that $\mathbf{E}[\bar{T}_n]$ is very close to zero even for small n (see the fifth column of Table II for remaining deviations). Note that, from its definition, the standard deviation of $\bar{T}_n$ is larger than that of $\bar{R}_n$ by a factor of $(1 - \gamma_n)^{-1} > 1$.

03 October 2023 09:46:41

TABLE II. Numerical estimation of the expected values $\mathbf{E}[\bar{R}_n]$ and $\mathbf{E}[\bar{T}_n]$. For each n, we generated $N = 10^9$ circular uniform random samples of size n. For each of the N samples, the values of $\bar{R}_n$ and $\bar{T}_n$ were then calculated. The sample means $\langle\bar{R}_n\rangle$ and $\langle\bar{T}_n\rangle$, used to estimate $\mathbf{E}[\bar{R}_n]$ and $\mathbf{E}[\bar{T}_n]$, were then calculated from the N values of $\bar{R}_n$ and $\bar{T}_n$. Only their significant digits are reported. The standard error (SE) of $\bar{R}_n$ (respectively, $\bar{T}_n$) is estimated by the sample standard deviation of $\bar{R}_n$ ($\bar{T}_n$) for the N observations. The standard error of $\langle\bar{R}_n\rangle$ (respectively, $\langle\bar{T}_n\rangle$) is $\text{SE}(\bar{R}_n)/\sqrt{N}$ ($\text{SE}(\bar{T}_n)$), with $1/\sqrt{N} = 3.16 \times 10^{-5}$. The low standard errors indicate that the expected values are closely approximated by $\langle\bar{R}_n\rangle$ and $\langle\bar{T}_n\rangle$. Note that the exact value of $\mathbf{E}[\bar{R}_2]$ is $2/\pi = 0.6366$ to four decimal places. Analogous tables in the supplementary material include results for all $n = 2, \ldots, 100$.

n	γ_n	$\langle\bar{R}_n\rangle$	$\langle\bar{R}_n\rangle - \gamma_n$	$\langle\bar{T}_n\rangle$	$\text{SE}(\bar{R}_n)$	$\text{SE}(\bar{T}_n)$
2	0.6267	0.6366	0.0100	0.0267	0.3078	0.8243
3	0.5117	0.5249	0.0132	0.0270	0.2405	0.4925
4	0.4431	0.4498	0.0067	0.0120	0.2184	0.3922
5	0.3963	0.4016	0.0053	0.0088	0.1967	0.3258
6	0.3618	0.3656	0.0038	0.0060	0.1816	0.2845
7	0.3350	0.3381	0.0031	0.0047	0.1690	0.2542
8	0.3133	0.3158	0.0025	0.0036	0.1589	0.2314
9	0.2954	0.2975	0.0021	0.0030	0.1503	0.2134
10	0.2802	0.2820	0.0018	0.0025	0.1430	0.1987
20	0.1982	0.1988	0.0006	0.0008	0.1024	0.1277
50	0.1253	0.1255	0.0002	0.0002	0.0652	0.0746
100	0.0886	0.0887	0.0001	0.0001	0.0462	0.0507
200	0.0627	0.0627	$<10^{-4}$	$<10^{-4}$	0.0327	0.0349
500	0.0396	0.0396	$<10^{-4}$	$<10^{-4}$	0.0207	0.0216
1000	0.0280	0.0280	$<10^{-4}$	$<10^{-4}$	0.0146	0.0151
2000	0.0198	0.0198	$<10^{-4}$	$<10^{-4}$	0.0104	0.0106
5000	0.0125	0.0125	$<10^{-4}$	$<10^{-4}$	0.0066	0.0066

REFERENCES

[1] K. V. Mardia and P. E. Jupp, *Directional Statistics* (Wiley, 2000).
[2] N. I. Fisher, *Statistical Analysis of Circular Data* (Cambridge University Press, 1995).
[3] S. R. Jammalamadaka and A. SenGupta, *Topics in Circular Statistics* (World Scientific Publishing, 2001).
[4] M. Hoke, K. Lehnertz, C. Pantev, and B. Lütkenhöner, "Spatiotemporal aspects of synergetic processes in the auditory cortex as revealed by the magnetoencephalogram," in *Brain Dynamics: Progress and Perspectives* (Springer, 1989), pp. 84–105.
[5] S. Aydore, D. Pantazis, and R. M. Leahy, "A note on the phase locking value and its properties," NeuroImage **74**, 231–244 (2013).
[6] W. A. Huang, I. M. Stitt, E. Negahbani, D. J. Passey, S. Ahn, M. Davey, M. Dannhauer, T. T. Doan, A. C. Hoover, A. V. Peterchev, S. Radtke-Schuller, and F. Fröhlich, "Transcranial alternating current stimulation entrains alpha oscillations by preferential phase synchronization of fast-spiking cortical neurons to stimulation waveform," Nat. Commun. **12**, 3151 (2021).
[7] P. A. Tass, M. G. Rosenblum, J. Weule, J. Kurths, A. Pikovsky, J. Volkmann, A. Schnitzler, and H. J. Freund, "Detection of n:m phase locking from noisy data: Application to magnetoencephalography," Phys. Rev. Lett. **81**, 3291–3294 (1998).
[8] J. P. Lachaux, E. Rodriguez, J. Martinerie, and F. J. Varela, "Measuring phase synchrony in brain signals," Hum. Brain Mapp. **8**, 194 (1999).
[9] F. Mormann, K. Lehnertz, P. David, and C. E. Elger, "Mean phase coherence as a measure for phase synchronization and its application to the EEG of epilepsy patients," Phys. Nonlinear Phenom. **144**, 358–369 (2000).
[10] C. A. Schevon, J. Cappell, R. Emerson, J. Isler, P. Grieve, R. Goodman, G. Mckhann, Jr., H. Weiner, W. Doyle, R. Kuzniecky, O. Devinsky, and F. Gilliam, "Cortical abnormalities in epilepsy revealed by local EEG synchrony," NeuroImage **35**, 140–148 (2007).
[11] P. J. Karoly, D. M. Goldenholz, D. R. Freestone, R. E. Moss, D. B. Grayden, W. H. Theodore, and M. J. Cook, "Circadian and circaseptan rhythms in human epilepsy: A retrospective cohort study," Lancet Neurol. **17**, 977–985 (2018).
[12] M. G. Leguia, R. G. Andrzejak, C. Rummel, J. M. Fan, E. A. Mirro, T. K. Tcheng, V. R. Rao, and M. O. Baud, "Seizure cycles in focal epilepsy," JAMA Neurol. **78**, 454–463 (2021).
[13] A. Espinoso and R. G. Andrzejak, "Phase irregularity: A conceptually simple and efficient approach to characterize electroencephalographic recordings from epilepsy patients," Phys. Rev. E **105**, 034212 (2022).
[14] B.-R. Choi, W. Jang, and G. Salama, "Spatially discordant voltage alternans cause wavebreaks in ventricular fibrillation," Heart Rhythm **4**, 1057–1068 (2007).
[15] J.-D. Janßen and T. Schanze, "Analysis and classification of ECG-waves and rhythms using circular statistics and vector strength," Curr. Dir. Biomed. Eng. **3**, 91–94 (2017).
[16] L. J. Vegosen, C. R. Weinberg, T. P. O'Hanlon, I. N. Targoff, F. W. Miller, and L. G. Rider, "Seasonal birth patterns in myositis subgroups suggest an etiologic role of early environmental exposures," Arthritis Rheumat. **56**, 2719–2728 (2007).
[17] S. Lamouille, E. Connolly, J. W. Smyth, R. J. Akhurst, and R. Derynck, "TGF-β-induced activation of mTOR complex 2 drives epithelial–mesenchymal transition and cell invasion," J. Cell Sci. **125**, 1259–1273 (2012).
[18] S. Kirschner and M. Tomasello, "Joint drumming: Social context facilitates synchronization in preschool children," J. Exp. Child Psychol. **102**, 299–314 (2009).
[19] P. Cook, A. Rouse, M. Wilson, and C. Reichmuth, "A California sea lion (*Zalophus californianus*) can keep the beat: Motor entrainment to rhythmic auditory stimuli in a non vocal mimic," J. Comp. Psychol. **127**, 412 (2013).
[20] A. Matsugaki, Y. Isobe, T. Saku, and T. Nakano, "Quantitative regulation of bone-mimetic, oriented collagen/apatite matrix structure depends on the degree of osteoblast alignment on oriented collagen substrates," J. Biomed. Mater. Res. **103**, 489–499 (2015).
[21] C. Rodrigues, M. Correia, J. M. C. S. Abrantes, M. A. B. Rodrigues, and J. Nadal, "Generalized lower limb joint angular phase space analysis of subject specific normal and modified gait," in *2018 40th Annual International Conference of the IEEE Engineering in Medicine and Biology Society (EMBC)* (IEEE, 2018), pp. 1490–1493.
[22] S. Fujita, M. Ohshima, and H. Iwata, "Time-lapse observation of cell alignment on nanogrooved patterns," J. R. Soc. Interface **6**, S269–S277 (2009).
[23] R. Kaunas, P. Nguyen, S. Usami, and S. Chien, "Cooperative effects of Rho and mechanical stretch on stress fiber organization," Proc. Natl. Acad. Sci. U.S.A. **102**, 15895–15900 (2005).
[24] J.-P. Hallier and D. Gaertner, "Drifting fish aggregation devices could act as an ecological trap for tropical tuna species," Mar. Ecol. Progr. **353**, 255–264 (2008).
[25] E. D. Wakefield, I. R. Cleasby, S. Bearhop, T. W. Bodey, R. D. Davies, P. I. Miller, J. Newton, S. C. Votier, and K. C. Hamer, "Long-term individual foraging site fidelity—Why some gannets don't change their spots," Ecology **96**, 3058–3074 (2015).
[26] H. Tatli, "Synchronization between the North Sea–Caspian pattern (NCP) and surface air temperatures in NCEP," Int. J. Climatol. **27**, 1171–1187 (2007).
[27] G. Villarini, "On the seasonality of flooding across the continental United States," Adv. Water. Resour. **87**, 80–91 (2016).
[28] M. Schimmel and H. Paulssen, "Noise reduction and detection of weak, coherent signals through phase-weighted stacks," Geophys. J. Int. **130**, 497–505 (1997).
[29] P. L. Read, X. Morice-Atkinson, E. J. Allen, and A. A. Castrejón-Pita, "Phase synchronization of baroclinic waves in a differentially heated rotating annulus experiment subject to periodic forcing with a variable duty cycle," Chaos **27**, 127001 (2017).
[30] I. Z. Kiss, Y. Zhai, and J. L. Hudson, "Emerging coherence in a population of chemical oscillators," Science **296**, 1676–1678 (2002).
[31] S. Nkomo, M. R. Tinsley, and K. Showalter, "Chimera and chimera-like states in populations of nonlocally coupled homogeneous and heterogeneous chemical oscillators," Chaos **26**, 094826 (2016).
[32] M. Ahmadi, A. R. H. Smith, and A. Dragan, "Communication between inertial observers with partially correlated reference frames," Phys. Rev. A **92**, 062319 (2015).

[33] A. Bergner, R. Meucci, K. Al Naimee, M. C. Romano, M. Thiel, J. Kurths, and F. T. Arecchi, "Continuous wavelet transform in the analysis of burst synchronization in a coupled laser system," Phys. Rev. E **78**, 016211 (2008).

[34] R. Donner and M. Thiel, "Scale-resolved phase coherence analysis of hemispheric sunspot activity: A new look at the north-south asymmetry," Astron. Astrophys. **475**, L33–L36 (2007).

[35] A. R. Taylor and P. Jagannathan, "Alignments of radio galaxies in deep radio imaging of ELAIS N1," Mon. Not. R. Astron. Soc. Lett. **459**, L36–L40 (2016).

[36] M. Frank, R. Biedert, E. Ma, I. Martinovic, and D. Song, "Touchalytics: On the applicability of touchscreen input as a behavioral biometric for continuous authentication," IEEE Trans. Inf. Forensics Secur. **8**, 136–148 (2012).

[37] U. Burgbacher and K. Hinrichs, "An implicit author verification system for text messages based on gesture typing biometrics," in *Proceedings of the SIGCHI Conference on Human Factors in Computing Systems* (ACM, 2014), pp. 2951–2954.

[38] Y. Kuramoto and D. Battogtokh, "Coexistence of coherence and incoherence in nonlocally coupled phase oscillators," Nonlinear Phenom. Complex Syst. **5**, 380–385 (2002).

[39] P. Clusella and R. Pastor-Satorras, "Phase transitions on a class of generalized Vicsek-like models of collective motion," Chaos **31**, 043116 (2021).

[40] L. Rayleigh, "XII. On the resultant of a large number of vibrations of the same pitch and of arbitrary phase," Philos. Mag. **10**, 73–78 (1880).

[41] E. García-Portugués and T. Verdebout, "An overview of uniformity tests on the hypersphere," arXiv:1804.00286 (2018).

[42] Y. Kuramoto, *Chemical Oscillations, Waves, and Turbulence* (Springer, 1984).

[43] B. Kralemann, A. Pikovsky, and M. Rosenblum, "Detecting triplet locking by triplet synchronization indices," Phys. Rev. E **87**, 052904 (2013).

[44] D. Naro, C. Rummel, K. Schindler, and R. G. Andrzejak, "Detecting determinism with improved sensitivity in time series: Rank-based nonlinear predictability score," Phys. Rev. E **90**, 032913 (2014).

[45] J. Arnhold, K. Lehnertz, P. Grassberger, and C. E. Elger, "A robust method for detecting interdependences: Application to intracranially recorded EEG," Phys. Nonlinear Phenom. **134**, 419–430 (1999).

[46] E. Ben-Jacob, S. Boccaletti, A. Pomyalov, I. Procaccia, and V. L. Towle, "Detecting and localizing the foci in human epileptic seizures," Chaos **17**, 043113 (2007).

[47] J. Prusseit and K. Lehnertz, "Measuring interdependences in dissipative dynamical systems with estimated Fokker-Planck coefficients," Phys. Rev. E **77**, 041914 (2008).

[48] J. Dauwels, E. Eskandar, and S. Cash, "Localization of seizure onset area from intracranial non-seizure EEG by exploiting locally enhanced synchrony," in *2009 Annual International Conference of the IEEE Engineering in Medicine and Biology Society* (IEEE, 2009), pp. 2180–2183.

[49] H. R. Zaveri, S. M. Pincus, I. I. Goncharova, R. B. Duckrow, D. D. Spencer, and S. S. Spencer, "Localization-related epilepsy exhibits significant connectivity away from the seizure-onset area," NeuroReport **20**, 891–895 (2009).

[50] G. Bettus, F. Wendling, M. Guye, L. Valton, J. Regis, P. Chauvel, and F. Bartolomei, "Enhanced EEG functional connectivity in mesial temporal lobe epilepsy," Epilepsy Res. **81**, 58–68 (2008).

[51] C. Rummel, M. Müller, G. Baier, F. Amor, and K. Schindler, "Analyzing spatio-temporal patterns of genuine cross-correlations," J. Neurosci. Methods **191**, 94–100 (2010).

[52] R. G. Andrzejak, D. Chicharro, K. Lehnertz, and F. Mormann, "Using bivariate signal analysis to characterize the epileptic focus: The benefit of surrogates," Phys. Rev. E **83**, 046203 (2011).

[53] R. G. Andrzejak, K. Schindler, and C. Rummel, "Nonrandomness, nonlinear dependence, and nonstationarity of electroencephalographic recordings from epilepsy patients," Phys. Rev. E **86**, 046206 (2012).

[54] N. P. Subramaniyam and J. Hyttinen, "Dynamics of intracranial electroencephalographic recordings from epilepsy patients using univariate and bivariate recurrence networks," Phys. Rev. E **91**, 022927 (2015).

[55] P. Klimeš, J. J. Duque, P. Jurák, J. Halámek, and G. A. Worrell, "Connectivity of epileptic brain regions in wake and sleep," in *2015 37th Annual International Conference of the IEEE Engineering in Medicine and Biology Society (EMBC)* (IEEE, 2015), pp. 2191–2194.

[56] R. S. Fisher, W. Van Emde Boas, W. Blume, C. Elger, P. Genton, P. Lee, and J. Engel, Jr., "Epileptic seizures and epilepsy: Definitions proposed by the International League Against Epilepsy (ILAE) and the International Bureau for Epilepsy (IBE)," Epilepsia **46**, 470–472 (2005).

[57] T. I. Netoff and S. J. Schiff, "Decreased neuronal synchronization during experimental seizures," J. Neurosci. **22**, 7297–7307 (2002).

[58] F. Wendling, F. Bartolomei, J. J. Bellanger, J. Bourien, and P. Chauvel, "Epileptic fast intracerebral EEG activity: Evidence for spatial decorrelation at seizure onset," Brain **126**, 1449–1459 (2003).

[59] K. Schindler, H. Leung, C. E. Elger, and K. Lehnertz, "Assessing seizure dynamics by analysing the correlation structure of multichannel intracranial EEG," Brain **130**, 65–77 (2007).

[60] K. Schindler, C. E. Elger, and K. Lehnertz, "Increasing synchronization may promote seizure termination: Evidence from status epilepticus," Clin. Neurophysiol. **118**, 1955–1968 (2007).

[61] C. Rummel, M. Goodfellow, H. Gast, M. Hauf, F. Amor, A. Stibal, L. Mariani, R. Wiest, and K. Schindler, "A systems-level approach to human epileptic seizures," Neuroinformatics **11**, 159–173 (2013).

[62] R. G. Andrzejak, C. Rummel, F. Mormann, and K. Schindler, "All together now: Analogies between chimera state collapses and epileptic seizures," Sci. Rep. **6**, 23000 (2016).

[63] P. Jiruska, M. De Curtis, J. G. R. Jefferys, C. A. Schevon, S. J. Schiff, and K. Schindler, "Synchronization and desynchronization in epilepsy: Controversies and hypotheses," J. Physiol. **591**, 787–797 (2013).

[64] W. Hoeffding, "A class of statistics with asymptotically normal distribution," Ann. Math. Stat. **19**, 293–325 (1948).

[65] M. Vinck, M. van Wingerden, T. Womelsdorf, P. Fries, and C. M. A. Pennartz, "The pairwise phase consistency: A bias-free measure of rhythmic neuronal synchronization," NeuroImage **51**, 112–122 (2010).

[66] R. Kutil, "Biased and unbiased estimation of the circular mean resultant length and its variance," Statistics **46**, 549–561 (2012).

[67] P. Celka, "Statistical analysis of the phase-locking value," IEEE Signal Process. Lett. **14**, 577–580 (2007).

[68] M. G. Leguia, V. R. Rao, J. K. Kleen, and M. O. Baud, "Measuring synchrony in bio-medical timeseries," Chaos **31**, 013138 (2021).

[69] Open access library repository, Universitat Pompeu Fabra; see https://doi.org/10.34810/data845.

[70] P. Chauvel, J. Gonzalez-Martinez, and J. Bulacio, "Presurgical intracranial investigations in epilepsy surgery," in *Handbook of Clinical Neurology* (Elsevier, 2019), Vol. 161, pp. 45–71.

[71] M. Bandarabadi, H. Gast, C. Rummel, C. Bassetti, A. Adamantidis, K. Schindler, and F. Zubler, "Assessing epileptogenicity using phase-locked high frequency oscillations: A systematic comparison of methods," Frontiers in Neurology **10**, 1132 (2019).